ChemComm

Accepted Manuscript

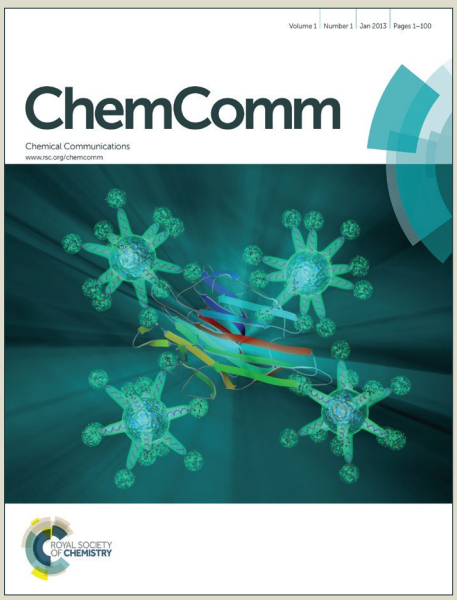

ROYAL SOCIETY OF CHEMISTRY

www.rsc.org/chemcomm

Journal Name

COMMUNICATION

Electrically Conducting Palladium Selenide (Pd_4Se, $Pd_{17}Se_{15}$, Pd_7Se_4) Phases: Synthesis and Activity Towards Hydrogen Evolution Reaction

Received 00th January 20xx,
Accepted 00th January 20xx

DOI: 10.1039/x0xx00000x

www.rsc.org/

Suresh Kukunuri, P. Muthu Austeria and S. Sampath*

Electrically conducting, continuous films of different phases of palladium selenides are synthesized by thermolysis of single source molecular precursors. The films on found to be adherent on flat substrates such as glass, indium tin oxide and glassy carbon and are stable under electrochemical conditions. They are electrocatalytically active and in particular, for hydrogen evolution reaction. Catalytic activities with low Tafel slopes of 50-60 mV/decade are observed.

Hydrogen, as a clean renewable energy source has attracted wide attention[1] and its global production primarily stems from steam reforming which requires methane and access to high temperatures.[2] In contrast, water electrolysis represents a clean, sustainable and environmentally friendly approach to generate H_2. Platinum is known to be the most efficient and commonly used electrocatalyst for hydrogen evolution reaction (HER).[3] Other metals from platinum group are also known to be good catalysts and are explored for various reactions involving organic synthesis, oxygen reduction reaction and photocatalysis.[4] Chalcogenides of palladium have attracted considerable attention in recent times and in particular the synthesis of various palladium sulphides and selenides have been reported.[5-9] Compositions of PdS and Pd_4S have been shown to exhibit good chemical stability and catalytic properties.[5] Similarly, palladium and selenium form different phases such as PdSe, $Pd_{17}Se_{15}$, Pd_7Se_4, Pd_4Se and $PdSe_2$ and various synthetic methods including solid state synthesis, solvothermal method, template assisted synthesis, thermal decomposition of complexes and hydrothermal method have been reported.[6-9]

Thermal decomposition of single molecular precursor is important among the synthetic routes because of its ease and use of relatively low temperatures.[7-9] O'Brien et al. have reported the synthesis of metal selenides based on low pressure chemical vapour deposition technique using platinum and palladium dithio/diselenoimido-diphosphinato complexes.[7] Jain et al. have reported the synthesis of palladium selenides by thermal decomposition of metal benzylselenolates, 2-(diethylamino)ethaneselenolates, monoselen-ocarboxylates and 2-(methoxycarbonyl)ethyl- selenolates complexes[8] and Singh et al. have explored the synthesis of palladium selenides from selenoether complexes of palladium.[9a] We have recently reported the use of didecylselenium based metal complexes to synthesize palladium selenides.[9b] Use of single source precursors to synthesize different phases of selenides is quite demanding as compared to solid state methods.[10]

Herein, we present the synthesis of various palladium selenides from the same palladium and selenium precursors containing different mole ratios by thermal decomposition. The films formed on glass substrates are well-characterized using electrical, microscopic and diffraction techniques. The electrocatalytic activity of palladium selenides have not been explored so far. It is found in the present studies, that they are excellent catalysts for driving electrochemical redox reactions and HER is used to exemplify this point.

Palladium selenide phases are obtained by thermolysis of palladium didecylselenium complexes. The complexes with different compositions are prepared by mixing different mole ratios of palladium acetate and didecyl selenide (DDSe) in toluene for 10 min. under ambient conditions. The Se precursor (DDSe) is synthesized by adopting a reported procedure.[11] In a typical synthetic procedure for the preparation of the complex, 40 µL of DDSe and 50 mg of $Pd(OAc)_2$ are stirred for 10 min, at 25°C. The complexes are represented as B_{xy}, where x and y denotes the moles of $Pd(OAc)_2$ and DDSe respectively. The complexes are drop-cast on freshly cleaned glass slides of 1 cm^2 area and the solvent evaporated under ambient conditions. Subsequently, the thermal decomposition of the complexes is carried out in a tubular furnace at 250°C for 1 h, under N_2 atmosphere resulting in the formation of stable, continuous and shiny black colored films. Different phase of palladium selenides are synthesized under different conditions and the details are tabulated in Table S1.

The palladium selenide films formed on the glass substrate are found to be very adherent and possess metallic shine with good electronic conductivity. The electrical resistivity values are found to be 30, 50 and 175 µΩcm for $Pd_{17}Se_{15}$, Pd_7Se_4 and Pd_4Se respectively. The thickness of the films range from few to several microns (2-7 µm) depending on the volume of the precursor complex used to cover the glass slide. The XRD patterns (Figure S1) of the precursor complex B_{11} on the glass surface shows diffraction peaks at 1.56 and 3.0° that correspond to (001) and (002) planes respectively and the appearance of periodic reflections is indicative of the formation of lamellar structure. The d-spacing values

Department of Inorganic and Physical Chemistry, Indian Institute of Science, Bangalore 560012, India. E-mail: sampath@ipc.iisc.ernet.in; Fax: +91-80-2360-0085; Tel: +91-80-2293-3315

† Electronic supplementary information (ESI) available: Detailed experimental procedures for the preparation of different palladium selenides,NMR,UV-Vis, XPS quantification, SEM images, XRD patterns of before and after stability

obtained for (001) and (002) planes are 56.6 and 29.3 Å that correspond to the bilayer formation of the complex from $Pd(OAc)_2$ and DDSe similar to the metal thiolates.[12] The formation of the complex is also evident from ^{77}Se NMR where a change in chemical shift value from 159 to 259 ppm is noted for the B_{11} complex as compared to pure Se. This may be attributed to a decrease in electron density on Se due to the co-ordination of its lone pair with Pd (Figure S2). The UV-Vis absorption spectra as a function of the molar ratios of $Pd(OAc)_2$ and DDSe (Figure S3) support the conclusions based on NMR and XRD. $Pd(OAc)_2$ and DDSe show absorption bands at 400 and 288 nm respectively. The absorption band obtained for $Pd(OAc)_2$ is due to the ligand to metal charge transfer transition while the band observed for DDSe is due to n to σ* transition (Figure S3a). The DDSe absorption band undergoes a bathochromic shift of 16 nm upon addition of varying amounts of $Pd(OAc)_2$ [Figure S3(b-c)]. Apart from this observation, disappearance of the band corresponding to $Pd(OAc)_2$ indicates the formation of the complex B_{1y}. It is reported that the reaction of $PdCl_2$ and didocosyl selenide results in the formation of complex of composition $Pd[(SeR_2)_2Cl_2]$.[13] Similarly, in the present study, the composition of the complex B_{1y} may be expected to be $Pd[(SeR_2)_2(OAc)_2]$, where the DDSe molecules bind via co-ordination bonds with Pd center through the lone pair of electrons present on Se atoms. Similarly, in the case of complex $B_{x1,}$ the composition is expected to be the same but with excess of $Pd(OAc)_2$. This is evident from the UV-Vis spectrum of the complex wherein the characteristic peak due to $Pd(OAc)_2$ observed at 400 nm increases with increasing amount of Pd precursor. This is absent in the case of the complex B_{1y} (Figure S3c).

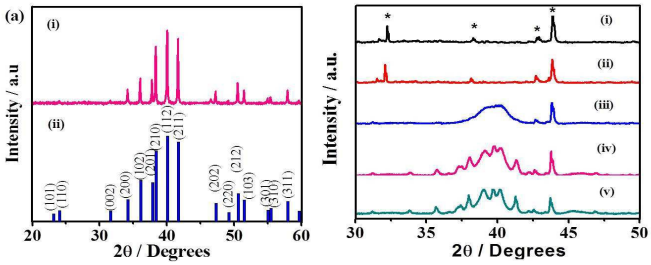

Figure 1. (a) X-ray diffraction patterns of (i) Pd_4Se prepared by the thermal decomposition of B_{41} complex at 250°C for 1 h in presence of N_2 and (ii) standard Pd_4Se pattern (JCPDF 73-1386). (b) In-situ XRD patterns of thermal decomposition of B_{41} complex at different temperatures (i) 25, (ii) 100, (iii) 150, (iv) 250 and (v) 350 °C. [* indicates peaks from the sample holder]

The phase identification of as-obtained materials formed by the thermal decomposition of B_{xy} is carried out using XRD. As shown in Figure S4, thermolysis of complex B_{11} at 250° C results in Pd_7Se_4 phase. The XRD pattern of Pd_7Se_4 corresponds to the orthorhombic system with lattice parameters, a = 5.23, b = 6.87 and c = 6.21 Å (JCPDF 31-0939). The crystallite size determined using Scherrer formula is ~ 76±5 nm. Similarly, the formation of the phase, Pd_4Se is observed at high mole ratio of palladium acetate in the complex, for instance B_{41}. The lattice parameters of pure Pd_4Se phase obtained are, a = 5.232 and c = 5.674 Å with tetragonal symmetry as given in Figure 1a. Further increase in the mole ratio of Se precursor in the complex results in the formation of $Pd_{17}Se_{15}$ phase (Fig. S4). The XRD pattern of $Pd_{17}Se_{15}$ reveals cubic phase with lattice parameter, a = 10.06 Å (JCPDF 73-1424). The crystallite size as determined using Scherrer formula is ~ 102±10 nm. The XRD patterns of the phases obtained from complexes B_{21} and B_{31} show the presence of peaks corresponding to both Pd_7Se_4 and Pd_4Se phases. Thus, the thermolysis of B_{11} and B_{41} yield pure Pd_7Se_4 and Pd_4Se phases respectively while the complexes B_{21} and B_{31} give mixed phases (Fig. S5). In order to get further insight into the evolution of palladium selenides, in-situ XRD patterns are recorded as a function of temperature. For instance, formation of pure phase of Pd_4Se is observed during the course of thermolysis of complex B_{41}. As shown in Figure 1b, the appearance of Pd_4Se phase is observed at 150°C and beyond.

The surface morphology of the Pd-selenides characterized using electron microscopy show continuous interconnected structures on glass slides (Figure S6). The energy dispersive x-ray analysis (EDX) shows the presence of palladium and selenium, along with small amount of carbon. The palladium to selenium ratios from EDX analysis nearly match with the corresponding phases. The Figure 2(a-c) shows the high resolution TEM images of $Pd_{17}Se_{15}$, Pd_7Se_4 and Pd_4Se phases. The respective d-spacing values calculated from the intensity line profiles are found to be 2.23, 2.64 and 3.19 Å that correspond to (112), (311) and (113) planes of the three phases. The d-spacing values are in agreement with the high intense reflections observed in the respective XRD patterns. Discrete spots observed in the SAED patterns indicate the crystalline nature of the materials (figure 2d-f).

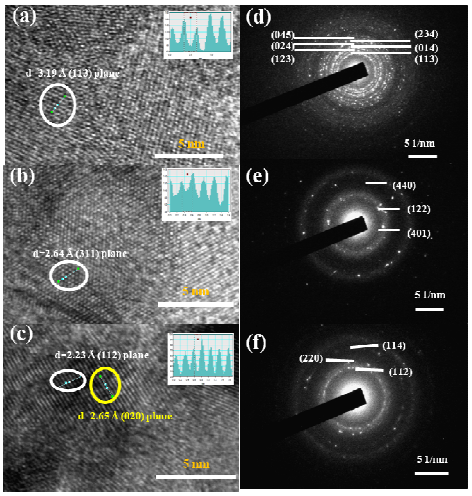

Figure 2. High resolution TEM images of (a) $Pd_{17}Se_{15}$, (b) Pd_7Se_4 and (c) Pd_4Se [inset in each image shows intensity line profile images] (d), (e) and (f) corresponding SAED patterns.

The chemical compositions as determined by the XPS are given in Table S2 and are close to the expected ratios. However, oxygen is also found to be present to a certain extent in the as-prepared material. This might be due to adventitious oxygen present on the surface during sample preparation and subsequent steps. The observation of randomly present carbon is likely to be due to the decomposition of alkyl chains in the palladium organoselenolate complex. High resolution spectra of Pd-3d and Se-3d are shown in Figure 3. The deconvolution of Pd-3d region displays a shift of 0.7 eV towards higher binding energies with respect to Pd (0) indicating the presence of residual positive charge on Pd in the case of Pd_7Se_4 phase. The binding energy (B.E) difference between Pd $3d_{5/2}$ and $3d_{3/2}$ is found to be 5.2 eV due to the spin-orbit coupling. The region corresponding to Pd-3p level overlaps with that of O1s region (Fig.S20). Once the sample is etched, the O1s peak is found to be absent indicating that the oxygen is adventitious in nature while others are retained in the same ratios (Fig. S21 & 22). The peaks corresponding to Se-3d shifts to lower B.E values as compared to that of Se (0), resulting in the residual negative charge on Se as

reported for many of metal selenides such as CoSe, NiSe and CuSe.[14] The Se-3d deconvoluted spectrum shows a spin-orbit coupling value of 0.8 eV. The XPS data for the other two phases, namely $Pd_{17}Se_{15}$ and Pd_4Se are shown in Figure 3 and Table S2. As observed, when Pd content increases from $Pd_{17}Se_{15}$ to Pd_4Se, the B.E values of Pd-3d peak shifts to lower values. The B.E values for Pd in $Pd_{17}Se_{15}$ (336.3 eV) does not exactly match with the Pd^0 (335.1 eV). The oxidation state of Pd is found to be between 0 and +2 in all three phases. The XPS spectra of palladium selenides are similar to other chalcogenides such as Pd_4S, PdS, PdSe and PdP.[14]

The palladium selenide phases prepared in the current study are highly conducting and possess work function values of ranging from 4.3 to 4.7 eV. Electrical resistivity measurements indicate that these phases are metallic in nature (Figure S8). Hence, they can act as

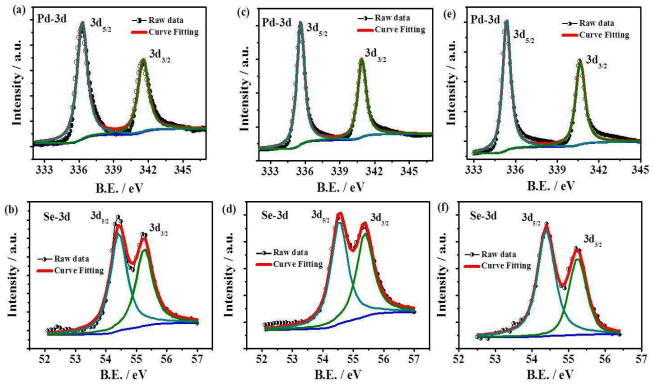

Figure 3. High resolution deconvoluted XPS spectra of Pd-3d and Se-3d regions of (a), (b) $Pd_{17}Se_{15}$, (c), (d) Pd_7Se_4 and (e), (f) Pd_4Se.

good electrode materials for driving redox reactions. Just to confirm the amenability of the materials for electrochemical studies, standard redox couple involving ferrocyanide / ferricyanide [Fe(II)/Fe(III)] has been studied in a standard three electrode cell. Figure S9a displays the cyclic voltammograms that reveal reversible peaks on the palladium selenide phases. Linear variation of peak currents with concentration of redox species is observed as well.

The electrocatalytic activity of palladium selenides towards HER has been followed using the as-obtained films on glass slides with copper wire as the contact. Polarization measurements are carried out in N_2-saturated 0.5M H_2SO_4 and the potentials are reported with respect to reversible hydrogen electrode (RHE, Figure S10). The IR corrected linear sweep voltammograms at 2 mV/sec scan rate, obtained using $Pd_{17}Se_{15}$, Pd_7Se_4 and Pd_4Se display onset potentials of -0.08, -0.07, -0.03 vs. RHE respectively (Figure S11a) for HER. Beyond the onset potential, the cathodic currents rise rapidly. Over potentials of -94 mV, -162 mV and -182 mV are observed to attain a current density of 10 mA/cm^2, for Pd_4Se, Pd_7Se_4 and $Pd_{17}Se_{15}$ respectively. In comparison to other well-known HER catalysts such as MoS_2, $MoSe_2$ and MoSSe,[15] the palladium selenide phases require low over potentials for hydrogen evolution. The adherence and stability of palladium selenide films towards continuous hydrogen evolution are improved considerably when Toray carbon paper (Figure S11) is used as the substrate. The presence of three dimensional fibrous carbon structures with roughness along with the high surface area of Toray carbon holds the selenides strongly and high HER activities can be obtained. Toray carbon itself is inactive towards HER (Figure S11b). The exchange current densities observed on Pt/C, Pd_4Se, Pd_7Se_4 and $Pd_{17}Se_{15}$ are 0.8 x 10^{-3} A/cm^2,[17] 2.3 x 10^{-4} A/cm^2, 2.5 x 10^{-5} A/cm^2 and 6.6 x 10^{-6} A/cm^2 respectively (Figure 4a). The apparent Tafel slopes are observed to be ~50, ~56 and ~57 mV per decade for Pd_4Se, Pd_7Se_4 and $Pd_{17}Se_{15}$ over 70- 100 mV over potentials, respectively, whereas the measured Tafel slope for Pt/C under identical conditions is 31 mV/dec (Figure 4b).[16] Tafel slopes are used only for comparing activity of different selenides.

The mechanism of H_2 evolution involves multi-step process[16] with the first step being the formation of H_{ads}.

$$H_3O^+ + e^- \longrightarrow H_{ads} + H_2O$$

Subsequently, the formation of H_2, may occur via one of the two different reaction pathways. First is the combination reaction (Tafel), in which two absorbed hydrogen atoms combine on the catalyst surface and other is based on the ion / atom reaction as given below (Heyrovsky step).

$$H_{ads} + H_{ads} \longrightarrow H_2$$

$$H_3O^+ + e^- + H_{ads} \longrightarrow H_2 + H_2O$$

Based on the Tafel slopes, it is likely that the HER mechanism probably follows Volmer - Heyrovsky steps in the case of the selenides. Among the three phases, Pd_4Se shows the lowest Tafel

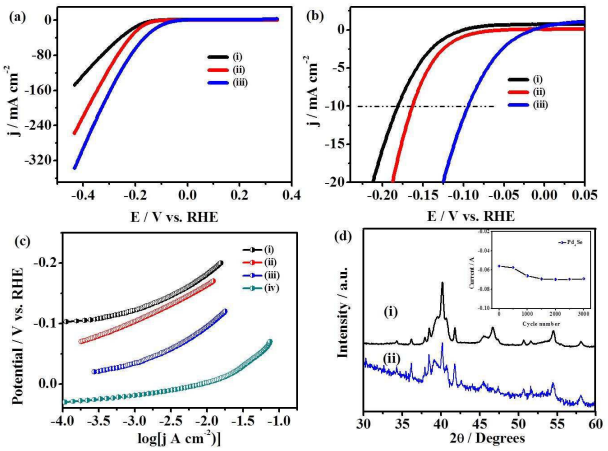

Figure 4 (a).IR corrected linear sweep voltammetric curves of (i) $Pd_{17}Se_{15}$, (ii) Pd_7Se_4 and (iii) Pd_4Se towards HER and (b) shows the enlarged portion of the onset potentials. (c) Tafel-plots for (i) $Pd_{17}Se_{15}$, (ii) Pd_7Se_4 and (iii) Pd_4Se (iv) Pt for catalysts loading of 0.28 mg/cm^2. Scan rate used is 2 mV/sec. (d) XRD patterns of Pd_4Se before (i) and after(ii) 3000 cycles, at a scan rate of 100 mV/s. Inset in figure d shows the stability of currents at -0.4 V as a function of cycling.

slope with highest exchange current density. The kinetic parameters obtained for the palladium selenide phases are better than the other known catalysts such as MoS_3 thin film (1.3 x 10^{-7} A/cm^2), MoS_2 nanoparticles (1.3-3.1 x 10^{-7} A/cm^2), FeP nanoparticles (1.7 x 10^{-5} A/cm^2) and Mo_2C bulk (3.79 x 10^{-6} A/cm^2).[18] The turnover frequency (TOF) values for Pd_4Se, Pd_7Se_4 and $Pd_{17}Se_{15}$ are determined to be 0.47 s^{-1}, 0.35 s^{-1} and 0.2 s^{-1} (at 0.05 V vs. RHE) respectively while the reported value for platinum is 0.9 s^{-1} (at 0 V vs. RHE). The TOF values of Pd-selenides are higher than that of Ni_2P (0.015 s^{-1}, at -100 mV vs. RHE) and MoS_2 (0.02 s^{-1}, at 0 V vs. RHE) (Table S3).[19] Figure S12 shows the impedance spectra along with the equivalent circuit used to fit the data. The R_{ct} values obtained are 86, 100 and 780 Ω for Pd_4Se, Pd_7Se_4 and $Pd_{17}Se_{15}$ respectively. Stability of the materials towards HER in 0.5M H_2SO_4 is checked by recording voltammetric i-v curves for 3000 continuous cycles between 0.25 and -0.4 V at 100 mV/s scan rate. Figure 4d and figure S14 show the variation of currents at different potentials as a function of number of scans. In general, the activity of

chalcogenides such as NiSe[19] are reported to decrease as a function of cycling while the palladium selenides are found to be very stable. The phase purity of the selenides after cycling for 3000 cycles is confirmed using SEM and XRD analyses (Figure S14,S15) and there is no significant change observed and the compositions of the phases remain unaltered after three thousand cycles of HER. The stability in alkaline conditions (1M KOH and 1M NaOH) has also been tested by cycling the electrode and checking the XRD patterns before and after the voltammetry studies. It is found that the phase purity is retained even after 1000 continuous cycles (Fig. S19). The XPS data confirm these observations on the stability of palladium selenide phases (Fig. S21). It is clear that any local, interfacial pH change that may occur during HER does not degrade the material. The activities of electrocatalysts also depend on the number of active sites for H-adsorption which in-turn depends on the electrochemical surface area of the material. The active surface areas of the three phases are determined using underpotential deposition of copper. The electrochemical surface areas of $Pd_{17}Se_{15}$, Pd_7Se_4 and Pd_4Se phases are found to be 0.048, 0.72 and 1 m^2/g respectively (Fig. S16).To understand and compare the activities of different phases of palladium selenides, density functional theory (DFT) calculations are carried out[20,21] and the details are given in the supporting information. The availability of d-band density of states (DOS) at the Fermi level is generally correlated with the electrocatalytic acivity[22]. It is found that the Pd d-band DOS are found to be higher and placed exactly above the fermi level in the case of Pd_4Se while in the other two cases, it is not (Figs. S17, S18). The selenium contribution at the Fermi level is found to be very small for Pd_4Se while it becomes fairly considerable in the case of the other two phases. Additionally, the positive charge on Pd (as given in XPS data earlier) is smaller in the case of Pd_4Se as compared to the other two, based on the shift in binding energy values (Table S2). The binding energy value for Pd (0) is 335.1 eV while the values are 335.3 eV for Pd_4Se and 336.3 and 336.7 eV for the other two phases. This is in parallel to the observation based on charge density analysis performed on the three selenides. The average charge on Pd is smaller in the case of Pd_4Se (0.05) and increases when the phases are Pd_7Se_4 (0.12) and subsequently $Pd_{17}Se_{15}$ (0.17) (Table S5). It should be noted that there are Pd atoms with different environment in the structures of the palladium selenides[23] and hence an average charge is given for comparative purposes. As a consequence, the oxidation state of Pd in Pd_4Se is smaller than that of the other two phases. This possibly will help in the effective adsorption of protons on Pd_4Se as compared to the Pd_7Se_4 and $Pd_{17}Se_{15}$. Of course, this is true when the adsorption sites are composed only of palladium. It is likely so since palladium (0) is a known hydrogen adsorption material. Additionally, the structural analysis reveals that the palladium sites are relatively open in the case of Pd_4Se and it is crowded as the composition becomes Pd_7Se_4 and $Pd_{17}Se_{15}$. All the above arguments lead to the fact that Pd_4Se is a better electrocatalyst than the other two members studied, Pd_7Se_4 and $Pd_{17}Se_{15}$. Low Tafel slope and charge transfer resistance and high exchange current density and electrochemical surface area makes Pd_4Se an excellent electrocatalyst as compared to the other two phases. An important point to highlight is the fact the adsorption / desorption peaks associated with of H atoms, before the onset of hydrogen gas evolution as observed on pure Pt and Pd phases is not observed in the case of palladium selenides. This requires further investigation.

In Summary, three different palladium selenide phases $Pd_{17}Se_{15}$, Pd_7Se_4 and Pd_4Se are prepared by thermolysis of different palladium organoselenolate complexes. Among the three phases, Pd_4Se shows very good electrocatalytic activity and this opens up ways of reducing the noble metal content in catalysts of interest.

Notes and references

1 N. S. Lewis and D. G. Nocera, *Proc. Natl. Acad. Sci. U. S. A.*, 2006, **103**, 15729.
2 N. R. Udengaard, *Prepr. Pap.-Am. Chem. Soc. Div. Fuel Chem.*, 2004, **49**, 906.
3 J. O. M. Bockris, I. A. Ammar and A. K. M. S. Huq, *J. Phys. Chem.*, 1957, **61**, 879.
4 (a) V. Ritleng, C. Sirlin and M. Pfeffer, *Chem. Rev.*, 2002, **102**, 1731; (b) B. Lim, M. Jiang, P. H. Camargo, E. C. Cho, J. Tao, X. Lu, Y. Zhu and Y. Xia, *Science*, 2009, **324**, 1302; (c) A. Kudo and Y. Miseki, *Chem. Soc. Rev.*, 2009, **38**, 253.
5 (a) L.-L. Long, A.-Y. Zhang, Y.-X. Huang, X. Zhanga and H.-Q. Yu, *J. Mater. Chem. A*, 2015, **3**, 4301; (b) Q. Chen, C. Suo, S. Zhang and Y. Wang, *Int. J. Photoenergy,* 2013, **2013**, 1.
6 (a) X. Jiang, B. Mayers, Y. Wang, B. Cattle and Y. Xia, *Chem. Phys. Lett.*, 2004, **385**, 472; (b) Madhu and R. N. Singh, *Int. J. Hyd. Energy*, 2011, **36**, 10006; (c) S. Geller, *Acta Crystallogr.*, 1962, **15**, 713; (d) M. Afzaal, M. A. Malik and P. O'Brien, *J. Mater. Chem.*, 2010, **20**, 4031.
7 P. L. Musetha, N. Revaprasadu, G. A. Kolawole, R. V. S. R. Pullabhotla, K. Ramasamy and P. O'Brien, *Thin Solid Films*, 2010, **519**, 197.
8 L. B. Kumbhare, V. K. Jain, P. P. Phadnis and M. Nethaji, *J. Organomet. Chem.*, 2007, **692**, 1546.
9 (a) H. Joshi, K. N. Sharma, A. K. Sharma, Om Prakash and A. K. Singh, *Chem. Commun.,* 2013, **49**, 7483; (b) K.Suresh, S N Karthick and S Sampath, *J.Mater.Chem A.,* 2015, DOI: 10.1039/c5ta04956c
10 H. R. Naren, A. Tamizhavel and S. Ramakrishan, *J. Phys.: Conf. Ser.*, 2011, **273**, 012074.
11 J. Muller and A. Terfort, *Inorg. Chim. Acta*, 2006, **359**, 4821.
12 N.S. John, G.U. Kulkarni, A. Datta, S.K. Pati, F. Komori, G. Kavitha, C. Narayana and M.K. Sanyal, *J. Phys. Chem. C*, 2007, **111**, 1868.
13 G. K. Rao, A. Kumar, B. Kumar and A. K. Singh, *Dalton Trans.*, 2012, **41**, 4306.
14 (a) A. B. Volynski, A. Yu. Stakheev, N. S. Telegina, V. G. Senin, L. M. Kustov and R. Wennrich, *Spectrochim. Acta Part B,* 2001, **56**, 1387; (b) V. V. Singh, U. Kumar, S. N. Tripathi and A. K. Singh, *Dalton Trans.*, 2014, **43**, 12555; (c) J. Zhang, Y. Xu and B. Zhang, *Chem. Commun.*, 2014, **50**, 13451.
15 (a) X. J. Bian, J. Zhu, L. Liao, M. D. Scanlon, P. Y. Ge, C. Ji, H. H. Girault and B. H. Liu, *Electrochem. Commun.*, 2012, **22**, 128; (b) V. Kiran, D. Mukherjee, R. N. Jenjeti and S. Sampath, *Nanoscale*, 2014, **6**, 12856.
16 Y. Li, H. Wang, L. Xie, Y. Liang, G. Hong and H. Dai, *J. Am. Chem. Soc.*, 2011, **133**, 7296.
17 (a) Y. Takasu, Y. Fujii, K. Yasuda, Y. Iwanaga and Y. Matsuda, *Electrochim. Acta*, 1989, **34***,* 453; (b) T. F. Jaramillo, K. P. Jorgensen, J. Bonde, J. H. Nielsen, S. Horch and I. Chorkendorff, *Science*, 2007, **317**, 100.
18 (a) D. Merki, S. Fierro, H. Vrubel, X. Hu, *Chemi. Sci.*, 2011, **2**, 1262; (b) J. D. Benck, Z. Chen, L.Y. Kuritzky, A.J. Forman, T.F. Jaramillo, *ACS Catal.*, 2012, **2**, 1916.
19 (a) Z. Zhang, B. Lu, J. Hao, W. Yang and J. Tang, *Chem. Commun.*, 2014, **50**, 11554; (b) C. He and J. Tao, *Chem. Commun.*, 2015, **51**, 8323; (c) E. J. Popczun, J. R. McKone, C. G. Read, A. J. Biacchi, A. M. Wiltrout, N. S. Lewis and R. E. Schaak, *J. Am. Chem. Soc.*, 2013, **135**, 9267.
20 G. Kresse and J. Furthmüller, *Phys. Rev. B*, 1996, **54**, 11169.
21 G. Kresse and D. Joubert, *Phys. Rev. B*, 1999, **59**, 1758.
22 A. Hamidani and B. Bennecer, *Comput. Mater. Sci.*, 2010, **48**, 115.
23 (a) T. Matkovic and K. Schubert, *J. Less-Common Met.*, 1978, **59**, 57; (b) F. Gronvold and E. Rost, *Acta. Crsytallogr.*, 1962, **15**, 11.